time tissue elastography, strain images are acquired and combined autocorrelation of echo signals generated before and after each compression (central frequency, 5.5 MHz; scanning rate, 360 lines/frame). Real-time tissue elastography is performed in B mode, whereas transient elastography is performed in A mode. As a result, real-time tissue elastography can be used to measure liver stiffness even in patients with ascites.

Second, for real-time tissue elastography, the compression needed for sonographic measurement is provided physiologically by spontaneous respiratory motion and vascular and cardiac pulsations. Thus only bare minimum compression with the linear probe is necessary for real-time tissue elastography, compared with the push pulse from the body surface required for transient elastography. In patients with ascites, the push pulse is prevented from reaching the liver parenchyma by the ascites. Real-time tissue elastography thus has more potential for precise evaluation of liver stiffness than does transient elastography.

We performed this prospective study with the participation of patients who were about to undergo radiofrequency ablation facilitated by artificial ascites. The results showed no significant difference in elastic ratios before and after injection for artificial ascites (Table 2). The differences in the noncirrhosis (p = 0.680) and cirrhosis (p = 0.980) groups were attributed to the heterogeneity of Metavir stage in the group without cirrhosis (all Metavir scores other than F4) compared with the cirrhosis group (Metavir score F4). The artificial ascites injected consisted of 5% glucose, differing from natural ascites fluid, which contains albumin, globulins, and electrolytes. To study differences between artificial ascites and natural ascites, we also performed real-time tissue elastography before and after treatments to control ascites in patients with cirrhosis who had natural ascites. The results showed that natural ascites, like artificial ascites, did not influence real-time tissue elastographic measurement (Table 3). Another problem for measurement with real-time tissue elastography is that liver stiffness can be measured within a depth of 5 cm. Because of the thickness of subcutaneous fat, however, the distance between the body surface and the liver has to be approximately 3 cm for precise measurement with this technique. If a patient has extreme ascites, real-time tissue elastography should be performed after ascites is controlled, shortening the distance between the body surface and the liver surface to within 3 cm. In such cases, stiffness of the left hepatic lobe can be evaluated, because less ascites is usually seen between the left lobe and the surface than between the right lobe and the surface. Otherwise, real-time tissue elastography with an endoscopic ultrasound probe can be considered [26, 27].

This study had limitations. Most of the patients enrolled had Metavir stage F4 disease, and no patient had F1 disease. The distribution of the patient sample was inappropriate for accurate assessment of fibrosis. The maximal distance between the body surface and the liver surface was 32.0 mm for real-time tissue elastography. For patients with a distance of 32.0 mm or more due to ascites or fat, a region of interest cannot be placed in the liver. This represents a mechanical limitation of real-time tissue elastography, and improvements in the hardware are required to address the issue.

Conclusion

Liver stiffness can be measured reproducibly with real-time tissue elastography even in patients with ascites. Because transient elastography cannot be used to evaluate liver stiffness in patients with cirrhosis and ascites, the real-time tissue elastographic method may have better potential than transient elastography for identification of liver stiffness. Moreover, real-time tissue elastography is noninvasive and is associated with less sampling error than liver biopsy and thus has advantages for both clinicians and patients when data on liver stiffness are needed to determine suitable treatment and evaluate prognosis.

References

1. Bravo AA, Sheth SG, Chopra S. Liver biopsy. *N Engl J Med* 2001; 344:495–500
2. Abdi W, Millan JC, Mezey E. Sampling variability on percutaneous liver biopsy. *Arch Intern Med* 1979; 139:667–669
3. Bedossa P, Dargere D, Paradis V. Sampling variability of liver fibrosis in chronic hepatitis C. *Hepatology* 2003; 38:1449–1457
4. Cadranel JF, Rufat P, Degos F. Practices of liver biopsy in France: results of a prospective nationwide survey. Group of Epidemiology of the French Association for the Study of the Liver (AFEF). *Hepatology* 2000; 32:477–481
5. Maharaj B, Maharaj RJ, Leary WP, et al. Sampling variability and its influence on the diagnostic yield of percutaneous needle biopsy of the liver. *Lancet* 1986; 1:523–525
6. Regev A, Berho M, Jeffers LJ, et al. Sampling error and intraobserver variation in liver biopsy in patients with chronic HCV infection. *Am J Gastroenterol* 2002; 97:2614–2618
7. Sandrin L, Tanter M, Gennisson JL, Catheline S, Fink M. Shear elasticity probe for soft tissues with 1-D transient elastography. *IEEE Trans Ultrason Ferroelectr Freq Control* 2002; 49:436–446
8. Sandrin L, Fourquet B, Hasquenoph JM, et al. Transient elastography: a new noninvasive method for assessment of hepatic fibrosis. *Ultrasound Med Biol* 2003; 29:1705–1713
9. Ziol M, Handra-Luca A, Kettaneh A, et al. Noninvasive assessment of liver fibrosis by measurement of stiffness in patients with chronic hepatitis C. *Hepatology* 2005; 41:48–54
10. Castera L, Vergniol J, Foucher J, et al. Prospective comparison of transient elastography, Fibrotest, APRI, and liver biopsy for the assessment of fibrosis in chronic hepatitis C. *Gastroenterology* 2005; 128:343–350
11. Ganne-Carrie N, Ziol M, de Ledinghen V, et al. Accuracy of liver stiffness measurement for the diagnosis of cirrhosis in patients with chronic liver diseases. *Hepatology* 2006; 44:1511–1517
12. Friedrich-Rust M, Ong MF, Martens S, et al. Performance of transient elastography for the staging of liver fibrosis: a meta-analysis. *Gastroenterology* 2008; 134:960–974
13. Fraquelli M, Rigamonti C, Casazza G, et al. Reproducibility of transient elastography in the evaluation of liver fibrosis in patients with chronic liver disease. *Gut* 2007; 56:968–973
14. Coco B, Oliveri F, Maina AM, et al. Transient elastography: a new surrogate marker of liver fibrosis influenced by major changes of aminotransferases. *J Viral Hepat* 2007; 14:360–369
15. Foucher J, Castera L, Bernard PH, et al. Prevalence and factors associated with failure of liver stiffness measurement using FibroScan in a prospective study of 2114 examinations. *Eur J Gastroenterol Hepatol* 2006; 18:411–412
16. Friedrich-Rust M, Ong MF, Herrmann E, et al. Real-time elastography for noninvasive assessment of liver fibrosis in chronic viral hepatitis. *AJR* 2007; 188:758–764
17. Wai CT, Greenson JK, Fontana RJ, et al. A simple noninvasive index can predict both significant fibrosis and cirrhosis in patients with chronic hepatitis C. *Hepatology* 2003; 38:518–526
18. Bedossa P, Poynard T. An algorithm for grading of activity in chronic hepatitis C. *Hepatology* 1996; 24:289–293
19. Kondo Y, Yoshida H, Shiina S, Tateishi R, Teratani T, Omata M. Artificial ascites technique for percutaneous radiofrequency ablation of liver cancer adjacent to the gastrointestinal tract. *Br J Surg* 2006; 93:1277–1282
20. Uehara T, Hirooka M, Ishida K. Percutaneous

ultrasound-guided radiofrequency ablation of hepatocellular carcinoma with artificially induced pleural effusion and ascites. *J Gastroenterol* 2007; 42:306–311

21. Saadeh S, Cammel G, Carey WD, Youmossi Z, Barns D, Easley K. The role of liver biopsy in chronic hepatitis C. *Hepatology* 2001; 33:196–200
22. Poynard T, Ratziu V, Bedossa P. Appropriateness of liver biopsy. *Can J Gastroenterol* 2000; 14: 543–548
23. French Metavir Cooperative Study Group. Intraobserver and interobserver variation in liver biopsy interpretation in patients with chronic hepatitis C. *Hepatology* 1994; 20:15–20
24. Afdhal NH. Diagnosing fibrosis in hepatitis C: is the pendulum swinging from biopsy to blood tests? *Hepatology* 2003; 37:972–974
25. Shiina T, Nitta N, Ueno E, Bamber JC. Real time tissue elasticity imaging using the combined autocorrelation method. *J Med Ultrasonics* 2002; 29:119–128
26. Giovannini M, Hookey L, Bories E, Pesenti C, Monges G, Delpero JR. Endoscopic ultrasound elastography: the first step towards virtual biopsy? Preliminary results in 49 patients. *Endoscopy* 2006; 38:344–348
27. Gheorghe L, Gheorghe C, Cotruta B, Carabela A. CT aspects of gastrointestinal stromal tumors: adding EUS and EUS elastography to the diagnostic tools. *J Gastrointestin Liver Dis* 2007; 16:346–347

Liver Fibrosis in Patients with Chronic Hepatitis C: Noninvasive Diagnosis by Means of Real-time Tissue Elastography—Establishment of the Method for Measurement[1]

Yohei Koizumi, MD
Masashi Hirooka, MD, PhD
Yoshiyasu Kisaka, MD, PhD
Ichiro Konishi, MD, PhD
Masanori Abe, MD, PhD
Hidehiro Murakami, MD, PhD
Bunzo Matsuura, MD, PhD
Yoichi Hiasa, MD, PhD
Morikazu Onji, MD, PhD

Purpose: To prospectively measure liver stiffness with real-time tissue elastography in patients with chronic hepatitis C and to compare the results with those of clinical assessment of fibrosis by using histologic stage as the reference standard.

Materials and Methods: All subjects gave informed consent, and the study was approved by the institutional ethics committee. Seventy hospitalized patients (46 men, 24 women; mean age, 65.5 years ± 11.7 [standard deviation]; age range, 33–87 years) with chronic hepatitis C underwent real-time elastography between January 2009 and September 2009. Elastography was performed at four liver locations by two independent observers. The elastic ratio (ratio of the value in the intrahepatic venous small vessels divided by the value in the hepatic parenchyma) was calculated and was compared with histologic fibrosis stage at liver biopsy. The elastic ratio and clinical fibrosis markers were assessed by using receiver operating characteristic (ROC) analysis. The differences between body site and observers were assessed with κ statistics and intraclass correlation coefficients (ICCs).

Results: Real-time tissue elastography cutoff values were 2.73 for F of 2 or greater, 3.25 for F of 3 or greater, and 3.93 for F of 4. No site differences were observed (κ = 0.835, ICC = 0.966), and the elastic ratio measurement was correlated between the two examiners (r^2 = 0.869, $P < .0001$). The areas under the ROC curves for elastic ratio, hyaluronic acid, type IV collagen, aspartate aminotransferase–to–platelet ratio index, FibroIndex, Forns score, and Hepascore were 0.95, 0.32, 0.73, 0.76, 0.76, 0.87, and 0.70, respectively; the elastic ratio performed better than the serum fibrosis markers and other scores.

Conclusion: Real-time tissue elastography is not invasive and could be used to evaluate liver fibrosis in patients with chronic hepatitis C.

Supplemental material: *http://radiology.rsna.org/lookup/suppl/doi:10.1148/radiol.10100319/-/DC1*

[1] From the Department of Gastroenterology and Metabology, Ehime University Graduate School of Medicine, Shitsukawa, Toon, Ehime 791-0295, Japan. Received February 9, 2010; revision requested March 24; revision received June 22; accepted July 13; final version accepted August 11. Supported by a Grant-in-Aid for Scientific Research (C) (Japan Society for the Promotion of Science, KAKENHI 21590848) and the Program for Enhancing Systematic Education in Graduate School from the Ministry of Education, Culture, Sports, Science and Technology, Tokyo, Japan. **Address correspondence to** Y.H. (e-mail: *hiasa@m.ehime-u.ac.jp*).

Chronic viral hepatitis infection increases liver fibrosis and stiffness and is an important cause of liver cirrhosis (1). Although liver biopsy is the reference standard for the diagnosis of liver fibrosis (2), it is an invasive procedure, which is difficult to perform in patients who need to be examined repeatedly to monitor the progression of liver fibrosis. Moreover, the evaluation of fibrosis with liver biopsy is associated with adverse events (3), sampling errors (4,5), and interpathologist and intrapathologist variabilities (6). Therefore, many studies have evaluated other noninvasive methods, such as the use of sonographic transient elastography (FibroScan; EchoSens, London, England) (7) and acoustic radiation force impulse (8) and laboratory tests, such as the aspartate aminotransferase-to-platelet ratio index, the FibroIndex, the Forns score, and the Hepascore, for the assessment of liver fibrosis stage.

Transient elastography is one of the techniques that can be used to evaluate mean tissue stiffness noninvasively (7). Results of several recent studies (9) have shown that measurements of liver stiffness with transient elastography are well correlated with fibrosis METAVIR stages. In addition, transient elastography is advantageous in that it can be repeatedly performed, does not require a highly experienced operator, and has a low risk of complications. However, there is a problem with reproducibility at identical measurement positions (10). In addition, it is not a real-time technique, because the image is not visible while the measurement is being taken. The reproducibility of transient elastography is also substantially reduced in patients with steatosis and increased body mass index (BMI) because the modality of ultrasonography (US) itself has limitations for visualizing the liver clearly in such patients (11).

Real-time tissue elastography is a relatively new method for the measurement of tissue elasticity. It uses a B-mode US machine, incorporating elastography into the conventional US scanner (12). In the previously reported technique, a US probe is used to slightly compress or relax the body (13), and the echo signals are captured in real time. This device calculates the relative hardness of tissue and displays this information as real-time color images (14); it can display tissue elasticity images and conventional B-mode images at the same time.

The purpose of this prospective study was to measure liver stiffness with real-time elastography in patients with chronic hepatitis C and to compare the results with those of other clinical assessments of fibrosis by using the histologic stage of fibrosis as the reference standard.

Advances in Knowledge

- In patients with hepatitis C, the areas under the receiver operating characteristic curves for prediction of fibrosis by means of elastic ratio, hyaluronic acid level, type IV collagen level, aspartate aminotransferase-to-platelet ratio index, FibroIndex, Forns score, and Hepascore were 0.95, 0.32, 0.73, 0.76, 0.76, 0.87, and 0.70, respectively, indicating that the elastic ratio performed better than the other serum fibrosis markers and scores.
- For METAVIR stages identified at histologic examination, real-time elastography cutoff values were 2.73 for F of 2 or greater, 3.25 for F of 3 or greater, and 3.93 for F of 4.
- Our results were independent of observer ($r^2 = 0.869$, $P < .0001$) and measurement positioning site (intraclass correlation coefficient: 0.966, $\kappa = 0.835$).

Implications for Patient Care

- Real-time elastography is not invasive and could be used to repeatedly evaluate liver fibrosis.
- Real-time elastography could be a powerful tool for time-course evaluation of liver cirrhosis during antiviral therapy.

Materials and Methods

Patients

The study protocol was approved by the institutional review board, and written informed consent was obtained. All enrolled patients underwent liver biopsy as part of the study. Seventy patients with chronic hepatitis C (mean age, 65.5 years ± 11.7 [standard deviation]; range, 33–87 years) were hospitalized in the Department of Gastroenterology and Metabology, Ehime University Hospital, Japan, from January 2009 to September 2009, and liver stiffness, which is related to the grade of liver fibrosis, was measured. Of the 70 patients, 46 were men (mean age, 63.5 years ± 13.9; range, 33–87 years), and 24 were women (mean age, 66.6 years ± 10.3; range, 46–84 years).

Inclusion criteria were the presence of hepatitis C virus (HCV) ribonucleic acid in serum according to real-time polymerase chain reaction and positive HCV antibody. The exclusion criteria were ascites (because that might interfere with measurements), coinfection with other viruses such as hepatitis B virus, other liver diseases such as primary biliary

Published online
10.1148/radiol.10100319

Radiology 2011; 258:610–617

Abbreviations:
AUC = area under the ROC curve
BMI = body mass index
CI = confidence interval
ICC = intraclass correlation coefficient
ROC = receiver operating characteristic
ROI = region of interest

Author contributions:
Guarantors of integrity of entire study, Y. Koizumi, M.H., Y. Kisaka, I.K., M.A., B.M., Y.H., M.O.; study concepts/study design or data acquisition or data analysis/interpretation, all authors; manuscript drafting or manuscript revision for important intellectual content, all authors; manuscript final version approval, all authors; literature research, Y. Koizumi, M.H., Y. Kisaka, I.K., M.A., B.M., Y.H.; clinical studies, Y. Koizumi, M.H., Y. Kisaka, I.K., M.A., H.M., B.M., Y.H.; experimental studies, Y. Koizumi, M.H., Y. Kisaka, I.K., M.A., Y.H.; statistical analysis, Y. Koizumi, M.H., Y. Kisaka, I.K., M.A., Y.H.; and manuscript editing, Y. Koizumi, M.H., Y. Kisaka, I.K., M.A., B.M., Y.H., M.O.

Authors stated no financial relationship to disclose.

Figure 1

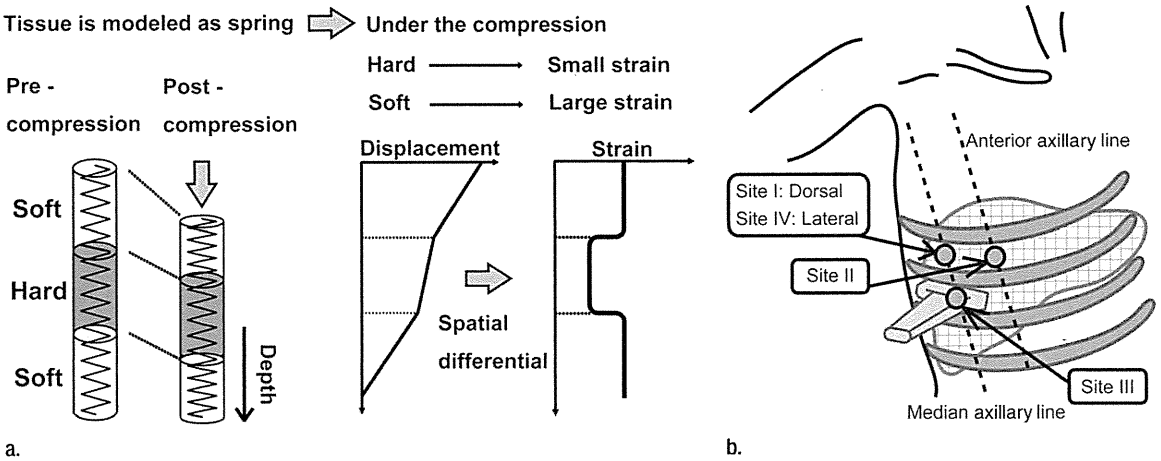

Figure 1: **(a)** The underlying method of real-time tissue elastography is the measurement and imaging of the strain distribution by adding the static pressure from the body surface; this is illustrated as a spring model. **(b)** The four measurement sites for real-time tissue elastography.

cirrhosis, and excessive alcohol consumption. (So that we could compare the METAVIR stages, which grade liver fibrosis only in patients with hepatitis C).

BMI and skin fold thickness were measured to determine whether they had any effects on real-time tissue elastography measurements.

Method for Measurement of Liver Stiffness

The underlining principle of real-time tissue elastography is illustrated in Figure 1a by using a spring model. When a spring is compressed, displacement in each section of the spring depends on the stiffness of the spring: A soft spring compresses more than a hard spring. The strain distribution, and in turn the stiffness in the spring, is measured by spatially differentiating the displacement at each location. On the basis of a previous report (13), we believed that compressing and relaxing the tissue with the US probe would be needed to measure the stiffness. However, we determined that we could measure the liver stiffness without adding any pressure from the probe because the liver itself receives pressure from the heartbeat automatically. Reflected US echoes are then used to compute the displacement and, thus, the strain distribution in the tissue. The examiners measured liver stiffness at four sites (Fig 1b), using the same positioning sites of the body as Boursier et al (10). The measurement sites were defined as follows: Site I was the dorsal decubitus and on the median axillary line and the first intercostal space; site II, the dorsal decubitus and on the anterior axillary line and the first intercostal space; site III, the dorsal decubitus and on the median axillary line and the second intercostal space; and site IV, the lateral decubitus and on the median axillary line and the first intercostal space. Real-time tissue elastography was performed five times at four measurement sites by two observers for each patient, in exhalation or inspiration to ensure that the liver was adequately depicted. The mean of the five measurements was calculated for comparison with histologic results.

Elastic Ratio

Hepatic elasticity was measured by using a US scanner with real-time tissue elastography (EUB-7500; Hitachi Medical Systems, Tokyo, Japan). We used a linear probe (EUP-L52; central frequency, 5.5 MHz). This scanner displays the color-coded elastography image overlaid on the B-mode image in real time (Fig 2a). Because this displayed color-coded elastography image shows only the relative tissue stiffness, a quantitative measuring technique called the elastic ratio was utilized.

The elastic ratio is the ratio of strain distribution in two selected regions of interest (ROIs). First, it was important to identify whether the hepatic vein or the portal vein would be a better internal control. We measured the value in the hepatic vein and portal vein for all 70 enrolled patients. The ROC curves of the elastic ratio calculated by using the ROI of the hepatic vein and the ROI of the portal vein as internal controls are shown in Figure 2b. The areas under the ROC curves (AUCs) of the elastic ratios obtained by using the hepatic vein as an internal control were higher than those obtained by using the portal vein as an internal control (intraclass correlation coefficient [ICC]: 0.953 [95% confidence interval {CI}: 0.903, 0.998] vs 0.731 [95% CI: 0.649, 0.886]; $P = .0006$). On the basis of the AUCs, the hepatic veins were used as an internal control. The ROI was placed on intrahepatic venous small vessels with a diameter of less than 3 mm and the hepatic parenchyma simultaneously. Subsequently, the ratio of the value in the intrahepatic venous small vessels was divided by the value in the hepatic parenchyma to generate the elastic ratio.

The elasticity of the hepatic vein was used as the reference because the elasticity of the veins does not change over time, since they do not undergo

Figure 2

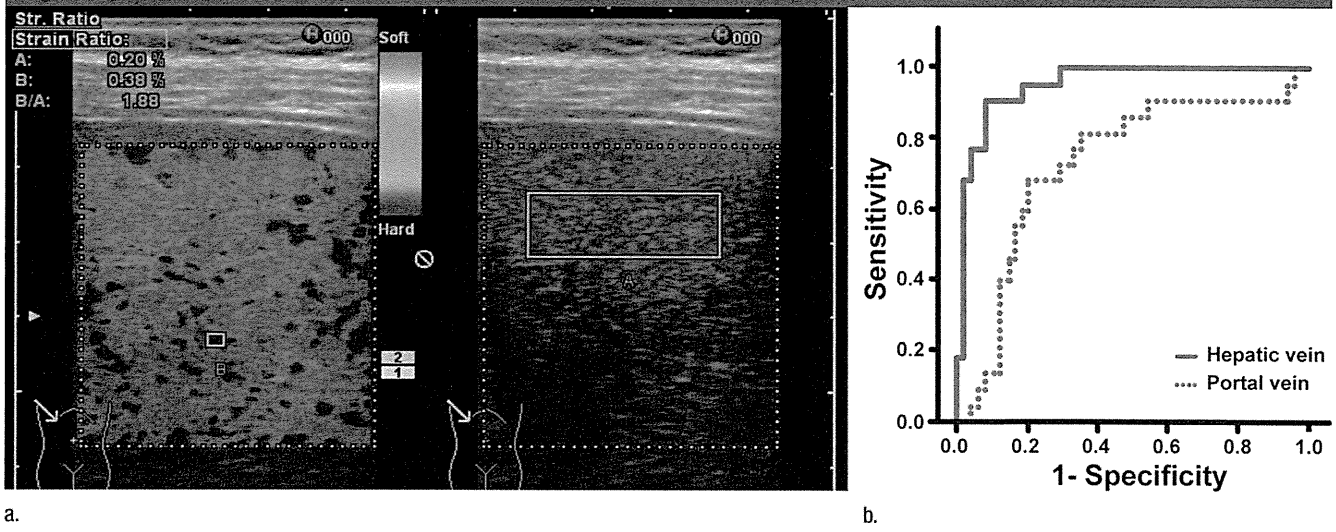

a. b.

Figure 2: **(a)** The elastic ratio is measured between the tissue compressibility of the liver (right) and that of the intrahepatic small vessel (left). Red indicates that tissue is soft, and blue indicates that it is hard. Information about displacement becomes the basis of the elastic information and is obtained by using a supersonic wave signal. **(b)** Receiver operating characteristic (ROC) curves of the elastic ratio obtained by using the hepatic vein or portal vein as an internal control.

transformations with disease, such as arteriosclerosis, and it also does not increase or decrease even when liver parenchyma becomes stiffer. Thus, small vessels with a diameter of 3 mm in the liver were used as the standard for computing the elasticity ratio, and the ROI was set as large as possible (usually 0.3 × 0.5 cm). The ROI in the liver parenchyma was placed 1 cm from the liver surface and was 2 × 1 cm in size. A higher elastic ratio indicates harder hepatic elasticity, corresponding to a higher stage of fibrosis. None of the patients had liver tumors in the measurement site that might have interfered with the real-time tissue elastography.

Observers

Two hepatologists (M.H. and Y. Koizumi, with 13 and 6 years of experience, respectively) performed the liver stiffness evaluation with real-time tissue elastography; each had already performed at least 100 liver stiffness evaluations (M.H., 350; Y. Koizumi, 120) prior to the beginning of the study. Each observer measured the elastic ratio five times at four sites (Fig 1b). The second observer was blinded to the results of the first observer. Measurement time for each measurement site (time from the beginning of measurement until completion to identify the elastic ratio with five measurements after placing the ROI) was recorded for each observer. For measurement site IV, the measurement time included the time for movement of the patient.

Liver Histologic Assessment

US-guided percutaneous liver biopsy (1.6-mm-diameter and 150-mm-long needle, suction technique) was performed within 1 week after hospitalization. Liver biopsy samples less than 12 mm long were excluded, because a sampling error for identifying liver fibrosis may occur with such samples (4). Liver biopsy samples were fixed in formalin and embedded in paraffin. Slices (4 μm thick) were stained with hematoxylin-eosin and impregnated with silver. Liver biopsies that contained fewer than five portal tracts (except for cirrhosis) were excluded from the histologic analysis. Fibrosis was staged by two pathologists (one of whom was I.K., with 16 years of experience), who were blinded to all patient characteristics. Fibrosis was staged on a four-point scale according to METAVIR (F0 indicated no fibrosis; F1, portal fibrosis without septa; F2, portal fibrosis and few septa; F3, numerous septa without cirrhosis; F4, cirrhosis) (15). Activity was graded according to METAVIR as A0, none; A1, mild; A2, moderate; and A3, severe (16). Lipid share was defined as mild, 0%–30%; moderate, 30%–60%; and severe, more than 60%.

Serum Fibrosis Markers

Levels of the following blood parameters were determined: aspartate aminotransferase, alanine aminotransferase, total bilirubin, platelets, gamma-glutamyl transferase, cholesterol, urea, hyaluronic acid, type IV collagen, cholinesterase, α1 and α2 globulins, β globulins, γ-globulins, prothrombin index, apolipoprotein-A1, haptoglobin, and ferritin. The aspartate aminotransferase (AST)–to–platelet ratio index (17) was calculated as follows: (AST/UNL · 100)/platelet count. (UNL is the upper limit of the normal aspartate aminotransferase.) The FibroIndex (18) was calculated as 1.738 − 0.064 (platelet count) + 0.005 (AST) + 0.463 (gamma-globulin). Forns score (19) was calculated as 7.811 − 3.131 ln(platelet count) + 0.781 ln(gamma-glutamyl transferase) + 3.467 ln(age) − 0.014 (cholesterol). Hepascore (20) was calculated as $y/(1 + y)$, $y = \exp[-4.185818 - (0.0249 \cdot \text{age}) + 0.7464 \cdot \text{sex}] + (1.0039 \cdot \alpha2\text{-macroglobulin}) + (0.0302 \cdot \text{hyaluronic acid}) + (0.0691 \cdot \text{bilirubin}) - (0.0012 \cdot \text{gamma-glutamyl transferase})$.

Statistical Analysis

The AUC of the elastic ratio was then compared with that derived from standard laboratory tests published in the literature, including the aspartate aminotransferase–to–platelet ratio index, FibroIndex, Forns score, and Hepascore (17–20). The ROC curve was prepared by using a statistical software package (JMP, version 8; SAS Institute Japan, Tokyo, Japan).

The diagnostic performance of liver stiffness evaluation and fibrosis was determined in terms of sensitivity, specificity, positive predictive value, negative predictive value, diagnostic accuracy, and AUC. The optimal cutoff values for liver stiffness were chosen to maximize the sum of sensitivity and specificity, and positive and negative predictive values were computed for those cutoff values.

Stiffness measurements were not normally distributed. Therefore, the elastic ratio was compared with the categories of the consensus fibrosis stage by using the Kruskal-Wallis nonparametric analysis of variance test. Correlations between the elastic ratio and the histologic fibrosis stage were also analyzed by using Spearman correlation coefficients.

The correlations between the values of each observer's real-time tissue elastography measurements, as well as the site differences, were evaluated by calculating κ coefficients and ICCs. The κ coefficient was defined as follows: poor, $\kappa < 0.4$; fair to good, $0.4 \leq \kappa < 0.75$; and excellent, $0.75 \leq \kappa$ (21). The ICC was defined as follows: slight, $0 \leq \text{ICC} < 0.20$; fair, $0.21 \leq \text{ICC} < 0.40$; moderate, $0.41 \leq \text{ICC} < 0.60$; substantial, $0.61 \leq \text{ICC} < 0.80$; and almost perfect, $\text{ICC} > 0.81$ (22).

The estimated sample sizes according to the two-sample Student *t* test in the F1–F3 group and F4 groups were 20 and 20 respectively, given a type I error of .05, a type II error of .2, and an effect size of 1.785. Multivariate stepwise logistic regression models were used to identify independent significant factors among serum fibrosis markers, METAVIR fibrosis stage, and activity grade, steatosis, BMI, and skin fold thickness for the elastic ratio determined with real-time tissue elastography. The statistical analyses were performed by using the JMP statistical software.

Table 1

Patient Characteristics

Characteristic*	All Patients ($n = 70$)	Men ($n = 46$)	Women ($n = 24$)
Age (y)	65.5 ± 11.7	66.6 ± 10.3	63.4 ± 13.9
BMI (kg/m²)	23.2 ± 3.37	22.8 ± 3.05	23.9 ± 3.82
ALT level (IU/L)	42.8 ± 31.4	46.3 ± 35.0	35.9 ± 21.9
Serum albumin level (g/dL)	3.68 ± 0.60	3.61 ± 0.61	3.81 ± 0.57
Platelet count ($10^4/\mu L$)	14.1 ± 7.12	14.1 ± 7.68	14.1 ± 6.05
Prothrombin time (%)	91.6 ± 18.1	89.3 ± 17.7	95.9 ± 18.4
Total bilirubin (mg/dL)	0.9 ± 0.44	0.95 ± 0.49	0.77 ± 0.30
GGT level (IU/L)	55.5 ± 46.8	62.6 ± 48.1	41.9 ± 41.6
Child-Pugh class			
A	63	40	23
B	7	6	1
C	0	0	0
Histologic fibrosis stage			
F1	12	6	6
F2	16	10	6
F3	19	12	7
F4	23	18	5
Histologic activity grade			
A0	1	1	0
A1	67	44	23
A2	2	1	1
A3	0	0	0
Histologic steatosis			
Mild	68	46	22
Moderate	2	0	2
Severe	0	0	0

Note.—Data are means ± standard deviations or numbers of patients.

* ALT = alanine aminotransferase, GGT = gamma-glutamyl transferase.

Results

Patients

Between January 2009 and September 2009, 70 patients met the inclusion criteria (Table 1). There were no significant differences in age ($P = .54$) or BMI ($P = .31$) between men and women. Gamma-glutamyl transferase was significantly higher in men ($P = .02$), but no significant difference was seen in the other biochemical tests between men and women (Table 1).

The rates of interobserver agreement in determining each fibrosis stage at each site were: site I, 81.4% (57 of 70 patients); site II, 71.4% (50 of 70 patients); site III, 74.3% (52 of 70 patients); and site IV, 75.7% (53 of 70 patients). For F4 or non-F4, the rate of interobserver agreement was: site I, 97.1% (68 of 70 patients); site II, 88.6% (62 of 70 patients); site III, 88.6% (62 of 70 patients); and site IV, 92.9% (65 of 70 patients). The mean κ value for F4 or non-F4 according to the elastic ratio was excellent at each site (site I, $\kappa = 0.94 \pm 0.04$ [standard error of the mean]; site II, $\kappa = 0.77 \pm 0.075$; site III, $\kappa = 0.77 \pm 0.08$; and site IV, $\kappa = 0.85 \pm 0.06$) (Table 2). At sites I–IV, the κ value, ICCs and 95% CIs indicated that the interobserver agreement was almost the same. The time for measurement was within 5 minutes for each measurement site, and the total measurement time for four sites was not significantly different between the two examiners ($P = .93$).

Table 2

Influence of Measurement Site on Interobserver Agreement

Parameter	Measurement Site				
	I	II	III	IV	All
ICC	0.95	0.92	0.91	0.94	0.97
95% CI	0.92, 0.97	0.87, 0.95	0.83, 0.93	0.90, 0.96	0.95, 0.98
Diagnosis of F1–F4 fibrosis (κ)	0.73	0.60	0.57	0.66	0.64
Diagnosis of F4 or non-F4 fibrosis (κ)	0.94	0.77	0.77	0.86	0.84
Measurement time for M.H. (min)	2.78 ± 1.38	2.92 ± 1.31	2.78 ± 1.38	3.12 ± 1.47	11.7 ± 1.66
Measurement time for Y. Koizumi (min)	2.82 ± 1.41	2.95 ± 1.29	2.77 ± 1.35	3.23 ± 1.41	11.9 ± 1.83

Figure 3

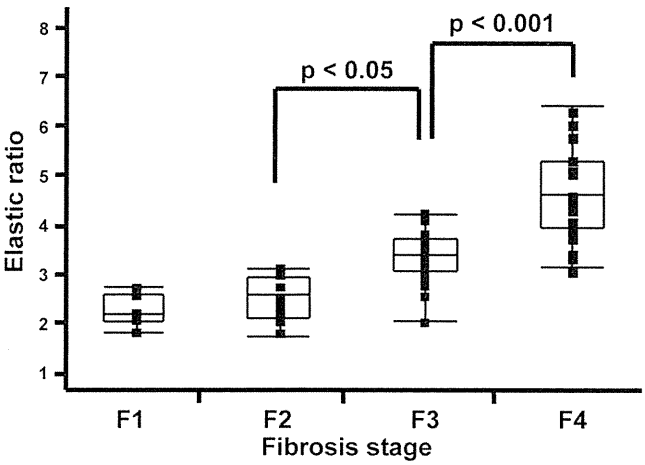

Figure 3: Graph shows elastic ratio for each fibrosis stage. The vertical axis is logarithmic scale. Tops and bottoms of the boxes = 1st and 3rd quartiles. The length of the box thus represents the interquartile range within which 50% of the values are located.

Figure 4

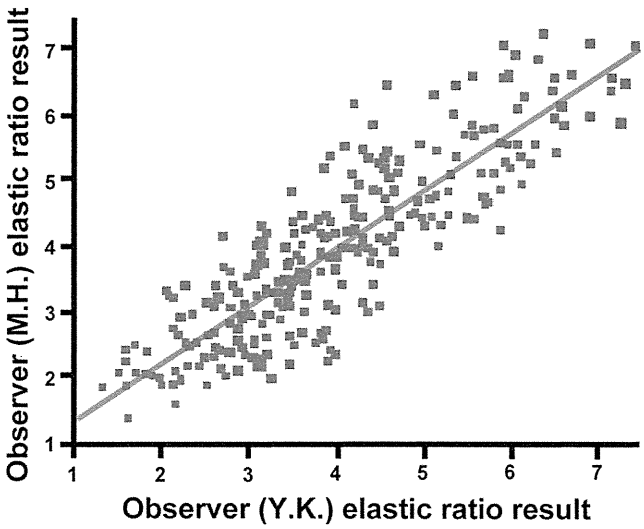

Figure 4: Graph shows correlation of elastic ratio measurement results between two examiners (Y. Koizumi and M.H., $r^2 = 0.869$, $P < .0001$).

Relationship between Liver Elastic Ratio and Histologic Parameters

The median value (95% CI) of the liver elastic ratio compared with the METAVIR fibrosis stage is shown in Figure 3: F1, 2.21 (1.94, 2.70); F2, 2.69 (2.29, 2.97); F3, 3.42 (3.07, 3.65); and F4, 4.66 (4.40, 4.93). The elastic ratios of each METAVIR fibrosis stage at liver biopsy differed significantly from each other (F2 vs F3, $r^2 = 0.36$, $P = .02$; F3 vs F4, $r^2 = 0.41$, $P < .001$). We found a significant correlation between fibrosis stage and the elastic ratio ($\rho = 0.82$, $P < .001$). However, there was no correlation between the METAVIR activity grade and the elastic ratio ($P = .36$). The elastic ratios identified by the two examiners were strongly correlated (Fig 4) and did not differ significantly. The optimal elastic ratio cutoff values obtained for the entire population, as well as the corresponding sensitivities and specificities, are shown in Table 3. The apparent cutoff values for F ≥ 2 (2.79) and F ≥ 3 (3.25) were close, but F ≥ 3 had higher sensitivity and specificity (85.4% and 96.4%) than F ≥ 2 (82.8% and 90.9%); however, the differences were not significant (sensitivity, $P = .67$; specificity, $P = .10$). A clear cutoff value (3.93) was obtained for F = 4, with sensitivity and specificity of 90.9% and 91.5%, respectively.

Mean real-time tissue elastography liver parenchyma values were as follows: site I, 0.07 ± 0.05 (standard deviation); site II, 0.08 ± 0.045; site III, 0.08 ± 0.06; site IV, 0.09 ± 0.05; and total, 0.08 ± 0.05 ($P = .09$). The mean absolute value of the hepatic vein vessels on real-time tissue elastography did not differ significantly according to site (site I, 0.25 ± 0.14; site II, 0.25 ± 0.12; site III, 0.26 ± 0.19; site IV, 0.25 ± 0.12; and total, 0.25 ± 0.13, $P = .94$).

Relationship between Liver Elastic Ratio and Fibrosis Blood Tests

The AUCs for diagnosis of fibrosis with elastic ratio, hyaluronic acid, type IV collagen (Fig 5a), aspartate aminotransferase–to–platelet ratio index, FibroIndex, Forns score, and Hepascore (Fig 5b) were 0.95, 0.32, 0.73, 0.76, 0.76, 0.87, and 0.70, respectively (Table 4). In the multivariate stepwise regression analysis, METAVIR fibrosis stage ($P < .0001$) and prothrombin time ($P = .0013$) were

Table 3

Elastic Ratio for Determination of METAVIR F Stage

Parameter	F ≥ 2 (F1 vs F2–F4)	F ≥ 3 (F1–F2 vs F3–F4)	F = 4 (F1–F3 vs F4)
AUC	0.89	0.94	0.95
Optimal cutoff	2.73	3.25	3.93
Sensitivity (%)	82.8	85.4	90.9
Specificity (%)	90.9	96.4	91.5
Positive predictive value (%)	98.0	97.2	83.3
Negative predictive value (%)	50.0	81.8	95.6

Table 4

Results of Comparison between Real-time Elastography and Fibrosis Blood Tests

Parameter	Real-Time Elastography	APRI*	Forns Score	FibroIndex	Hepascore
AUC	0.95	0.76	0.87	0.76	0.70
Sensitivity (%)	90.9	81.8	68.2	63.6	63.4
Specificity (%)	91.5	74.4	95.8	87.5	70.8

* APRI = aspartate aminotransferase–to–platelet ratio index.

Figure 5

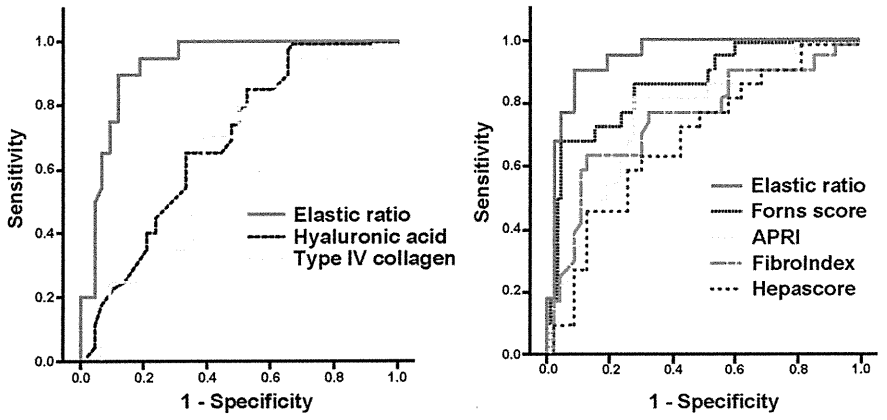

Figure 5: **(a, b)** ROC curves for diagnosis of liver fibrosis (F4) with real-time elastography. The AUC for the diagnosis of clinically important liver fibrosis or cirrhosis (F4) by using the EUB-7500 (Hitachi Medical Systems) device is superior to the results with **(a)** blood parameters or **(b)** calculated fibrosis indexes. *APRI* = aspartate aminotransferase–to–platelet ratio index.

independently associated with the elastic ratio.

Skin Fold Thickness and BMI

Interobserver agreement for elastic ratio was excellent when the skin fold thickness was less than 20 mm and BMI was less than 25 kg/m^2. However, for patients with a skin fold thickness greater than 20 mm or a BMI greater than 25 kg/m^2, the interobserver agreement was not as good (Table 5).

Discussion

There are many reports and approaches to evaluating liver stiffness without liver biopsy. Among them, the FibroScan appears useful (23,24), but there are few reports about its reproducibility. Boursier et al (10) reported that the reproducibility of the liver hardness measurement obtained by using the FibroScan differs according to measurement position. Since the absolute value of liver stiffness at real-time tissue elastography was variable, we established a procedure to obtain reproducibility by using the signal of the small hepatic veins as a reference. Using the elastic ratio, we found no difference in reproducibility for four measurement positions. Moreover, real-time tissue elastography has other advantages compared with the FibroScan or the acoustic radiation force impulse (Appendix E1 [online]).

We checked the reproducibility of the elastic ratio derived from real-time tissue elastography. The real-time tissue elastography procedure reported previously (13) involves applying pressure in the intercostal space with a probe; thus, when the pressure applied with the probe differs, the real-time tissue elastography value changes. This means that the value of liver stiffness differs not only with each observer, but also within the same observer. Therefore, we put a probe in the intercostal space and conducted the examination with no added pressure, because when observers add pressure during measurement, observer bias may occur. The liver itself receives pressure from the heartbeat automatically, so the elastic ratio could be measured without adding any pressure with the probe. Thus, observer variability can be lessened with this procedure.

Fatty change of the liver affects the evaluation of liver stiffness with the FibroScan (11). We performed a multivariate stepwise regression analysis to identify factors that affect real-time tissue elastography. Skin fold thickness, BMI, and liver steatosis were not identified as factors affecting the elastic ratio determined by using real-time tissue elastography, while fibrosis stage was a factor. Therefore, real-time tissue elastography may measure the degree of fibrosis. Only for patients with a skin fold thickness greater than 20 mm or BMI greater than 25 kg/m^2 did the interobserver agreement have a wider range, though the difference was not significant (perhaps owing to the small

Table 5

Results according to BMI and Skin Fold Thickness

Parameter	Group 1	Group 2	Group 3	Group 4	Group 5
BMI (kg/m^2)	<19 (n = 5)	≥19 To <22 (n = 21)	≥22 To <25 (n = 27)	≥25 To <28 (n = 9)	≥28 (n = 8)
ICC	0.91	0.94	0.90	0.88	0.88
95% CI	−0.39, 1.0	0.81, 0.98	0.77, 0.96	0.36, 0.94	0.39, 0.98
Skin fold thickness (mm)	<15 (n = 15)	≥15 To <20 (n = 37)	≥20 To <25 (n = 13)	≥25 (n = 5)	...
ICC	0.95	0.92	0.83	0.81	...
95% CI	0.83, 0.98	0.84, 0.96	0.51, 0.95	−0.68, 1.00	...

sample size). The elastic ratio could be calculated for the two patients with BMIs greater than 30 kg/m^2. Further studies involving more severely obese individuals will be needed to confirm the usefulness of real-time tissue elastography for such patients.

The elastic ratio obtained by using real-time tissue elastography performed better than serum fibrosis markers and scores of fibrotic change based on blood laboratory tests. However, our study still had limitations. It is difficult to evaluate certain types of patients with B mode US, including those with thick, fat tissue under the skin; a history of abdominal operations; difficulty stopping breathing; too much liver atrophy; or a large amount of ascites. We had only two observers, each with experience with the modality, and used only one US machine. Therefore, our results might not be applicable to other individuals with less experience. Our cutoffs for determination of accuracy were based on our own results and therefore are likely overestimates of performance.

In summary, in patients with chronic hepatitis C, real-time tissue elastography allows for noninvasive assessment of fibrosis that does not vary with the sites we tested or by observer and performs better than fibrosis indexes calculated by using blood laboratory tests.

Acknowledgments: The authors thank Ravi Managuli, PhD, RDMS (Department of Bioengineering, University of Washington, Seattle, Wash), for assistance in editing the technical comments and Yoshiko Soga, MD, PhD (Pathology Division, Ehime University Hospital, Ehime, Japan), for evaluating the histologic features of liver specimens.

References

1. Lauer GM, Walker BD. Hepatitis C virus infection. N Engl J Med 2001;345(1):41–52.
2. Strader DB, Wright T, Thomas DL, Seeff LB; American Association for the Study of Liver Diseases. Diagnosis, management, and treatment of hepatitis C. Hepatology 2004; 39(4):1147–1171. [Published correction appears in Hepatology 2004;40(1):269.]
3. Cadranel JF, Rufat P, Degos F. Practices of liver biopsy in France: results of a prospective nationwide survey. For the Group of Epidemiology of the French Association for the Study of the Liver (AFEF). Hepatology 2000;32(3):477–481.
4. Pagliaro L, Rinaldi F, Craxì A, et al. Percutaneous blind biopsy versus laparoscopy with guided biopsy in diagnosis of cirrhosis: a prospective, randomized trial. Dig Dis Sci 1983;28(1):39–43.
5. Regev A, Berho M, Jeffers LJ, et al. Sampling error and intraobserver variation in liver biopsy in patients with chronic HCV infection. Am J Gastroenterol 2002;97(10):2614–2618.
6. Rousselet MC, Michalak S, Dupré F, et al. Sources of variability in histological scoring of chronic viral hepatitis. Hepatology 2005;41(2):257–264.
7. Sandrin L, Fourquet B, Hasquenoph JM, et al. Transient elastography: a new noninvasive method for assessment of hepatic fibrosis. Ultrasound Med Biol 2003;29(12): 1705–1713.
8. Friedrich-Rust M, Ong MF, Martens S, et al. Performance of transient elastography for the staging of liver fibrosis: a meta-analysis. Gastroenterology 2008;134(4):960–974.
9. Friedrich-Rust M, Wunder K, Kriener S, et al. Liver fibrosis in viral hepatitis: noninvasive assessment with acoustic radiation force impulse imaging versus transient elastography. Radiology 2009;252(2):595–604.
10. Boursier J, Konaté A, Gorea G, et al. Reproducibility of liver stiffness measurement by ultrasonographic elastometry. Clin Gastroenterol Hepatol 2008;6(11):1263–1269.
11. Fraquelli M, Rigamonti C, Casazza G, et al. Reproducibility of transient elastography in the evaluation of liver fibrosis in patients with chronic liver disease. Gut 2007;56(7): 968–973.
12. Yamakawa M, Nitta N, Shiina T, et al. High-speed freehand tissue elasticity imaging for breast diagnosis. Jpn J Appl Phys 2003;42: 3265–3270.
13. Friedrich-Rust M, Ong MF, Herrmann E, et al. Real-time elastography for noninvasive assessment of liver fibrosis in chronic viral hepatitis. AJR Am J Roentgenol 2007; 188(3):758–764.
14. Shiina T. Real time tissue elasticity imaging using the combined autocorrelation method. J Med Ultrason 1999;26(2):57–66.
15. Intraobserver and interobserver variations in liver biopsy interpretation in patients with chronic hepatitis C. The French METAVIR Cooperative Study Group. Hepatology 1994; 20(1 pt 1):15–20.
16. Bedossa P, Poynard T. An algorithm for the grading of activity in chronic hepatitis C. The METAVIR Cooperative Study Group. Hepatology 1996;24(2):289–293.
17. Wai CT, Greenson JK, Fontana RJ, et al. A simple noninvasive index can predict both significant fibrosis and cirrhosis in patients with chronic hepatitis C. Hepatology 2003;38(2):518–526.
18. Koda M, Matunaga Y, Kawakami M, Kishimoto Y, Suou T, Murawaki Y. FibroIndex, a practical index for predicting significant fibrosis in patients with chronic hepatitis C. Hepatology 2007;45(2):297–306.
19. Forns X, Ampurdanès S, Llovet JM, et al. Identification of chronic hepatitis C patients without hepatic fibrosis by a simple predictive model. Hepatology 2002;36(4 pt 1): 986–992.
20. Adams LA, Bulsara M, Rossi E, et al. Hepascore: an accurate validated predictor of liver fibrosis in chronic hepatitis C infection. Clin Chem 2005;51(10):1867–1873.
21. Fleiss JL. Statistical methods for rates and proportions. 2nd ed. New York, NY: Wiley, 1981;218.
22. Landis JR, Koch GG. The measurement of observer agreement for categorical data. Biometrics 1977;33(1):159–174.
23. Harada N, Soejima Y, Taketomi A, et al. Assessment of graft fibrosis by transient elastography in patients with recurrent hepatitis C after living donor liver transplantation. Transplantation 2008;85(1):69–74.
24. Fraquelli M, Rigamonti C. Diagnosis of cirrhosis by transient elastography: what is hidden behind misleading results. Hepatology 2007;46(1):282; author reply 282–283.

Clinical Translational Research

Oncology

Oncology 2011;80:406–415
DOI: 10.1159/000330734

Received: April 19, 2011
Accepted after revision: June 15, 2011
Published online: August 15, 2011

Identification by Differential Tissue Proteome Analysis of Talin-1 as a Novel Molecular Marker of Progression of Hepatocellular Carcinoma

Hideaki Kanamori[a, b] Takao Kawakami[d, e] Kathryn Effendi[b] Ken Yamazaki[b] Taisuke Mori[b] Hirotoshi Ebinuma[a] Yohei Masugi[b] Wenlin Du[b] Keiko Nagasaka[e] Atsushi Ogiwara[e] Yutaka Kyono[e] Minoru Tanabe[c] Hidetsugu Saito[a] Toshifumi Hibi[a] Michiie Sakamoto[b]

Departments of [a]Gastroenterology, [b]Pathology and [c]Surgery, School of Medicine, Keio University, [d]Clinical Proteome Center, Tokyo Medical University, and [e]Research and Development Division, Medical ProteoScope Company, Tokyo, Japan

Key Words

Tumor progression · Liquid chromatography-tandem mass spectrometry · Immunohistochemistry · Portal vein invasion · Disease-free survival

Abstract

Objective: Hepatocellular carcinoma (HCC) is characterized by a multistage process of tumor progression. This study addressed its molecular features to identify novel protein candidates involved in HCC progression. ***Methods:*** Using liquid chromatography-tandem mass spectrometry, proteomes of 4 early HCCs and 4 non-HCC tissues derived from 2 cases of liver transplant surgery were compared with respect to the separation profiles of their tryptic peptides. Immunohistochemistry was performed on 106 HCC nodules to confirm the results of the proteomic analysis. ***Results:*** Statistical analysis of the profiles selected the peptide peaks differentiating HCC from non-HCC. A database search of the tandem mass spectrometry data from those peptide peaks identified 61 proteins, including a cytoskeletal protein, talin-1, as upregulated in HCC. Talin-1 expression levels in HCC nodules were significantly associated with the dedifferentiation of HCC ($p = 0.001$). A follow-up survey of the examined clinical cases revealed a correlation between talin-1 upregulation and a shorter time to recurrence after resection ($p = 0.039$), which may be related to the higher rate of portal vein invasion in HCCs with talin-1 up-regulation ($p = 0.029$). ***Conclusions:*** Proteomic analysis led to identification of talin-1 as a promising HCC marker. Talin-1 upregulation is associated with HCC progression and may serve as a prognostic marker.

Introduction

Hepatocellular carcinoma (HCC), like other cancers, is characterized by a multistage process of tumor progression [1]. In the initial stage, the damaged liver tissues evolve into small nodular hypercellular lesions called dysplastic nodules (DNs). These precancerous lesions develop into early HCC, defined as small, well-differentiated HCC of vaguely nodular type, and then into progressed HCC, characterized by a distinctly nodular appearance and frequent microvascular invasion. After treatment, early HCC has a longer time to recurrence and a higher 5-year survival rate than progressed HCC [2]. The long-standing confusion in differentiating early HCC from high-

KARGER

Fax +41 61 306 12 34
E-Mail karger@karger.ch
www.karger.com

0030–2414/11/0806–0406$38.00/0

Accessible online at:
www.karger.com/ocl

Michiie Sakamoto, MD, PhD
Department of Pathology
School of Medicine, Keio University
35 Shinanomachi, Shinjuku-ku, Tokyo 160-8582 (Japan)
Tel. +81 3 5363 3764, E-Mail msakamot@sc.itc.keio.ac.jp

grade DN has been minimized since stromal invasion was recognized as a diagnostic indicator for early HCC [3], but hepatocellular changes occurring during malignant transformation are still not well characterized.

Transcriptomic and proteomic analyses are useful techniques for investigating the carcinogenesis of several malignant diseases. Comparison of the gene expression profiles among early and progressed components of nodule-in-nodule type HCCs and corresponding noncancerous liver tissues resulted in identification of heat-shock protein 70 (HSP70) [4] and cyclase-associated protein 2 [5] as molecular markers of HCC. In this study, we performed proteome analysis for direct comparison of the protein composition of early HCC and non-HCC tissues obtained from whole native livers of patients who underwent living donor liver transplantation (LDLT). During the last decade, liquid chromatography (LC) directly coupled with tandem mass spectrometry (MS/MS) has been widely used for high-resolution proteome-wide analysis from a complex protein mixture [6]. The use of an improved LC-MS/MS technology with optimal tissue sampling led us to the identification of a variety of proteins up-regulated in HCC, including talin-1.

Talin-1 is a cytoskeletal protein with a molecular mass of 270 kDa, and has been shown to play a key role in a wide variety of integrin-mediated cellular events [7]. To our knowledge, there has been no report published on the relationship between talin-1 and HCC. We have successfully applied a proteomic approach to native livers of LDLT cases and showed up-regulation of talin-1 during HCC progression.

Materials and Methods

Liver Samples

HCC and noncancerous liver tissues were obtained from HCC patients at Keio University Hospital between 2003 and 2006. This study was conducted with the approval of the Ethics Committee of Keio University School of Medicine. For proteomic analysis, we used fresh whole livers from 2 HCC patients who received LDLT. Both patients had similar clinical backgrounds (males, 49 and 54 years old at the time of surgery, infected with hepatitis C virus) and were referred to Keio University Hospital after transarterial chemoembolization for multiple HCCs and hepatic deterioration into Child-Pugh score C. Immediately after resection of the whole liver, physiological saline including 2,000 units of heparin sodium was infused into the catheterized portal trunk. After confirming visually that the fluid flowing out of the common hepatic artery and the hepatic veins did not contain residual blood, the liver was sliced into 1.5-cm-thick sections with reference to the magnetic resonance imaging. Two samples of early HCC and 2 samples of noncancerous liver tissue were macroscopically separated in 0.5–1.0-cm^3 portions from each of the livers by two experienced pathologists. The noncancerous samples were derived from the areas which were not adjacent to cancerous lesions and did not contain many fibrotic components. A total of 8 liver samples (4 HCCs and 4 noncancerous tissues) were obtained from the 2 cases and kept frozen at −80°C until use. For immunohistochemical analysis, liver samples were obtained by partial hepatectomy or liver transplant surgery, consisting of 106 HCC nodules (13 well-differentiated HCCs including 7 early, 73 moderately differentiated, and 20 poorly differentiated HCCs) and 8 DNs from the total of 91 HCC patients.

Two-Dimensional Liquid Chromatography (2DLC)-MS/MS

The resected tissues were homogenized, and the homogenates were fractionated into phosphate-buffered saline (PBS) soluble and insoluble fractions [8]. An aliquot (50 μg protein) of the soluble fraction was subjected to tryptic hydrolysis in a polyacrylamide gel matrix [8, 9]. The resulting peptide mixture was extracted from the gel matrix and dried under vacuum. Peptide separation and mass measurement were carried out using 2DLC-MS/MS [10]. Briefly, in the first-dimensional strong cation exchange (SCX) LC, the peptides retained in the SCX LC column were eluted by successive injection of ammonium formate solutions (25, 50, 100, 150, 200 and 500 mM). These effluents were mixed serially with an internal standard peptide mixture consisting of 3 synthetic peptides. The second-dimensional reverse-phase (RP) LC was performed in a total 60-min acetonitrile gradient for each of the SCX LC peptide effluents. The RP LC effluent was interfaced with an electrospray ionization source in positive ion mode on an LTQ linear ion trap mass spectrometer (Thermo Fisher Scientific Inc., Waltham, Mass., USA). Protonated peptides were analyzed sequentially for MS/MS in Data-Dependent Scanning mode, consisting of a full-range scan at an m/z range of 450–2,000 and subsequent product ion scans for each of the three most intense ions in the full scan mass spectrum.

Differential Analysis of Peptide Profiles

A peptide separation profile, consisting of the ion signals characterized by RP LC elution time, full scan m/z value and full scan signal intensity was extracted from each of the RP LC-MS/MS data files. Profile compilation was carried out using an in-house program as reported [11]. Here, the signal alignment process was aided by three common signal sets derived from the three peptides spiked into each SCX LC effluent. Following signal alignment, peak detection was performed by searching the compiled signal profile. The intensity of each detected peak is the total of the signal intensities provided from the respective peptide profiles. Student's t test and heat map representation were performed for the ion signals contained in the detected peaks using Spotfire® software (TIBCO Software Inc., Palo Alto, Calif., USA).

For peptide identification, a database search was performed using Mascot® software (Matrix Science Ltd., London, UK) [12]. MS/MS data were searched for corresponding amino acid sequences in a Swiss-Prot database (http://expasy.org/sprot). Each peptide identification item was computationally associated with a profile peak containing the original precursor ion signals. Peptide identifications were considered significant for a Mascot matching score greater than 30. Identified amino acid sequences of peptides were searched for in the Swiss-Prot database to count the identical sequences in the database.

After selection of the peptide identifications under given conditions, these were grouped into each Swiss-Prot protein sequence entry. According to the fold value of signal intensity, these peptide groups were evaluated for quantitative regulation of the corresponding protein molecules. Functional classification of these proteins was based on information described in the Gene Ontology database (http://www.geneontology.org/).

Immunohistochemistry

Immunohistochemical staining was performed on formalin-fixed, paraffin-embedded tissue sections as described previously [13]. Each section was deparaffinized, rehydrated, incubated with fresh 0.3% hydrogen peroxide in methanol for 30 min at room temperature, and then washed in PBS. The sections were autoclaved at 120°C in 10 mM sodium citrate, pH 6.0, for 10 min before incubation with normal horse serum (Vector Laboratories Inc., Burlingame, Calif., USA) for 30 min. The sections were then incubated with a mouse monoclonal antibody against talin-1 (clone TA205; Millipore Co., Billerica, Mass., USA) at a dilution of 1:200 overnight at 4°C, washed with PBS, and incubated with a secondary antibody for 60 min at room temperature. Staining was evaluated by 3 pathologists. Statistical analyses were performed using SAS® software (SAS Institute Inc., Cary, N.C., USA). Disease-free survival curves were calculated from the day of resection using the Kaplan-Meier method (JMP® software, SAS Institute), and the significance of differences in survival rates between the patient groups was calculated by the log-rank test. The results of the immunohistochemical examination were compared with the microarray data of our past study [14] which are accessible from the Genome Medicine Database of Japan (GeMDBJ; https://gemdbj.nibio.go.jp/dgdb/index.do).

Results

Differential Proteome Analysis of the Compiled Peptide Profiles

From each of the 8 liver samples, 2DLC-MS/MS generated 6 peptide profiles for each of 6 salt concentrations of SCX LC (fig. 1a). The profile compilation was performed separately for each set of 6 SCX LC fractions across the 8 tissue samples, followed by peak detection of the compiled signals. From the 6 SCX LC fractions above, we obtained 2,434, 1,912, 1,819, 1,894, 1,725, and 1,533 peaks, respectively, associated with any peptide identifications. All 11,317 peaks were subjected to selection on the basis of the following conditions: (1) A Student's t test p value less than 0.1 for difference of the signal intensities between HCC and non-HCC. (2) At least 1 peptide identification, with a Mascot matching score more than 30, associated with the relevant peak. (3) Peak intensity more than 1% of the maximum peak in a compilation. After selection, the number of candidate peaks was reduced to 283, comprising 390 peptide identifications, allowing more than two significant peptide identifications in each of the selected peaks. The heat map of the 283 peaks shows successful differentiation between HCC and non-HCC (fig. 1b).

Evaluation and Classification of Tumor Marker Candidates for HCC

Following peak selection, 390 peptide identifications associated with the selected peaks were grouped according to the protein names. Of these, 288 peptide identifications were assigned to 111 groups (proteins), whereas the remaining 102 were individual peptides supported by only single peptide identification from one sample. The latter were excluded from the following analysis because of their ambiguity both for identification and quantitation of protein. According to the fold value, i.e. the ratio of HCC to non-HCC on the average signal intensities involved in a peak, these 111 peptide groups were evaluated for the quantitative regulation status of the corresponding protein molecules. When peptides with a greater than 1-fold value accounted for more than 80% in a peptide group, the corresponding protein was considered to be upregulated in HCC. A total of 61 proteins fell into this category. Accounting for less than 20% of the total, 22 proteins were categorized as downregulated. The other 28 groups were not categorized into either set. The 61 upregulated and 22 downregulated proteins were classified further by their functional and topological aspects, based on the Gene Ontology annotations as follows (table 1): 8 cytoskeletal proteins, 7 heat shock proteins (including HSP70 as upregulated in HCC), 5 major blood proteins, 53 enzymes, and 10 other proteins.

Among several categories of proteins, we primarily chose the cytoskeletal proteins for further validation, since it is generally accepted that disorders in cellular morphogenesis underpinned by the cytoskeleton are associated with tumor progression [15], and many papers addressing cytoskeletal proteins as tumor markers have been published recently [5, 16, 17]. Table 2 focuses on the six cytoskeletal proteins which we identified as upregulated in HCC: actin α/β, filamin-A, talin-1, tubulin α chain, tubulin β chain, and WD repeat-containing protein 1. Actin was identified from 3 peptides significantly upregulated in HCC, and these peptides, SYELPDGQ-VITIGNER, QEYDESGPSIVHR and IW-HHTFYNELR, are affiliated with 10, 5 and 7 genes, respectively, of the actin isoforms according to the Swiss-Prot database. Accordingly, the peptide identifications were unable to distinguish among these isoforms. This also is the case for identification of the tu-

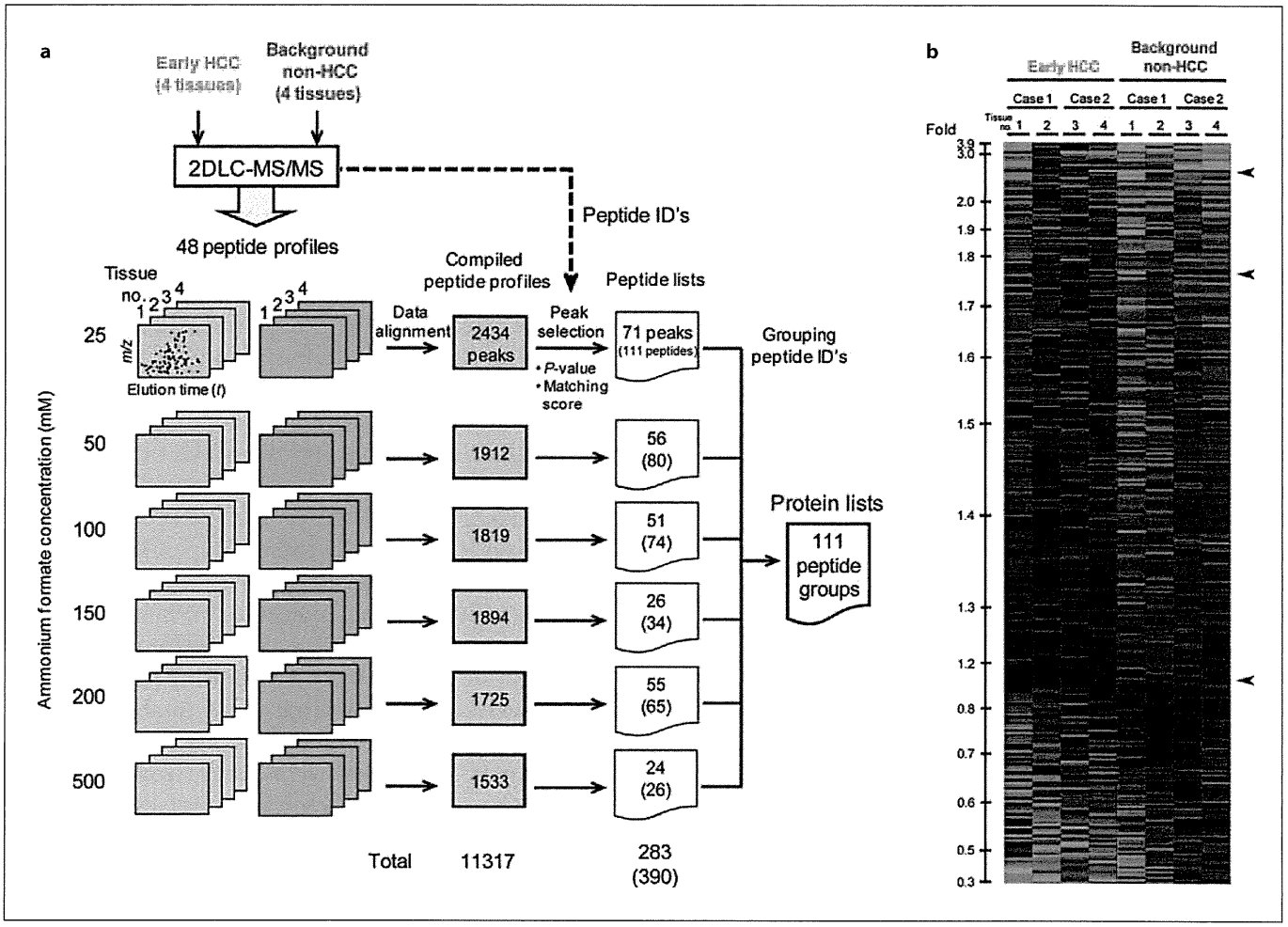

Fig. 1. Proteomic differential analysis using 2DLC-MS/MS. **a** 2DLC-MS/MS of an individual sample generated 6 peptide profiles from SCX LC peptide fractions. The profile data were compiled separately for each SCX LC fraction. This illustration shows the numbers of peaks and peptide identifications in each step. **b** Heat map representation of the 283 peptide peaks. Each color patch represents the ion signal intensity scaled to the mean of signal intensities in the corresponding peptide peak, as a continuum of relative intensity levels from green (less than 0.25-fold of the mean) to bright red (more than 2.5-fold of the mean). These peak data are shown in descending order of the fold value of early HCC to non-HCC. Arrowheads indicate the peak containing a talin-1-derived peptide.

Table 1. Classification of the candidate proteins for HCC tumor marker

Classification	Upregulated	Downregulated	Total
Cytoskeletal protein	6	2	8
Heat shock protein	6	1	7
Major blood protein	3	2	5
Enzyme	39	14	53
Others	7	3	10
Total	61	22	83

Proteins were identified from the peptides whose ion intensities varied significantly between early HCCs and non-HCC tissues ($p < 0.1$). The fold values of early HCC to non-HCC for the peptide ion intensities were used to evaluate the quantitative regulation status of the individual proteins in early HCC.

Table 2. Cytoskeletal proteins upregulated in early HCC

Protein identity (molecular weight, kDa)	Amino acid sequence of peptide	SCX LC salt concentration mM	Mascot ion score[a]	Fold value[b]	p value[c] $\times 10^2$	Swiss-Prot accession (gene name[d])	Number of Swiss-Prot accessions[e]
Actin (42)	SYELPDGQVITIGNER	25	46	1.4	8.95	A5A3E0 (A26C1B), P60709 (ACTB), P62736 (ACTA2), P63261 (ACTG1), P63267 (ACTG2), P68032 (ACTC1), P68133 (ACTA1), Q562R1 (ACTBL2), Q6S8J3 (A26C1A), Q9BYX7 (FKSG30)	10
	QEYDESGPSIVHR	100	35	1.6	2.16	A5A3E0 (A26C1B), P60709 (ACTB), P63261 (ACTG1), Q6S8J3 (A26C1A), Q9BYX7 (FKSG30)	5
	IWHHTFYNELR	200	38	1.4	9.56	A5A3E0 (A26C1B), P60709 (ACTB), P63261 (ACTG1), P68032 (ACTC1), P68133 (ACTA1), Q6S8J3 (A26C1A), Q9BYX7 (FKSG30)	7
Filamin-A (280)	IVGPSGAAVPCK	25	61	1.2	7.10	P21333 (FLNA)	1
Talin-1 (270)	LNEAAAGLNQAATELVQASR	25	35	2.4	3.71	Q9Y490 (TLN1)	1
	VQELGHGCAALVTK	50	35	1.2	4.34	Q9Y490 (TLN1)	1
	LASEAKPAAVAAENEEIGSHIK	100	54	1.7	8.37	Q9Y490 (TLN1)	1
Tubulin α chain (50)	AVFVDLEPTVIDEVR	25	81	1.9	8.43	P68363 (TUBA1B), Q71U36 (TUBA1A), Q9BQE3 (TUBA1C)	3
	AVFVDLEPTVIDEIR	100	70	2.0	2.64	P68366 (TUBA4A)	1
	LISQIVSSITASLR	100	64	1.3	6.70	P68363 (TUBA1B), P68366 (TUBA4A), Q9BQE3 (TUBA1C), Q9H853 (TUBA4B), Q9NY65 (TUBA8)	5
	IHFPLATYAPVISAEK	150	42	1.2	9.75	P68363 (TUBA1B), P68366 (TUBA4A), Q13748 (TUBA3C), Q6PEY2 (TUBA3E), Q71U36 (TUBA1A), Q9BQE3 (TUBA1C)	6
Tubulin β chain (50)	YLTVAAVFR	25	72	1.5	9.68	P04350 (TUBB4), P07437 (TUBB), P68371 (TUBB2C)	3
	SGPFGQIFRPDNFVFGQS GAGNNWAK	200	83	2.3	2.30	P04350 (TUBB4), P07437 (TUBB), P68371 (TUBB2C), Q13885 (TUBB2A), Q9BVA1 (TUBB2B)	5
WD repeat-containing protein 1 (66)	IKDIAWTEDSKR	150	45	1.3	6.76	O75083 (WDR1)	1

[a] The score (S) given as $S = -10 \times \log_{10}(P)$, where P is the absolute probability that the observed match between the MS/MS data and the amino acid sequence is a random event (http://www.matrixscience.com). [b] Signal intensity ratio of early HCC to non-HCC. [c] Significance of the difference between the ion signal intensities of early HCC and non-HCC. [d] The extract from each of the protein entries in Swiss-Prot database of Release 56.1 of September 2, 2008. [e] Protein entries containing the corresponding amino acid sequence.

bulin α and β chains, where the identified peptide sequences belong to 1 or more tubulin isoforms. Identifications of filamin-A and WD repeat-containing protein 1 were supported only by single amino acid sequences. Talin-1 was identified from 3 amino acid sequences, LNEAAAGLNQAATELVQASR, VQELGHGCAALVTK and LASEAKPAAVAAENEEIGSHIK, each being unique in the database. The relevant fold values were 2.4, 1.2 and 1.7, respectively. We focused on talin-1 because of the low ambiguity in both the identification and up-regulation. The real-time quantitative reverse transcription-polymerase chain reaction (RT-PCR) analysis of 3 LDLT cases, including the 2 cases used for the proteomic analysis, also revealed upregulation of talin-1 mRNA in HCC compared to noncancerous liver (data not shown).

Talin-1 Expression in HCC Tissue Samples

The early HCC nodules used for proteomic analyses were stained by the anti-talin-1 antibody with obvious intensity (fig. 2a). Compared with Kupffer cells, vascular smooth muscle cells, bile duct and sinusoidal endothelial

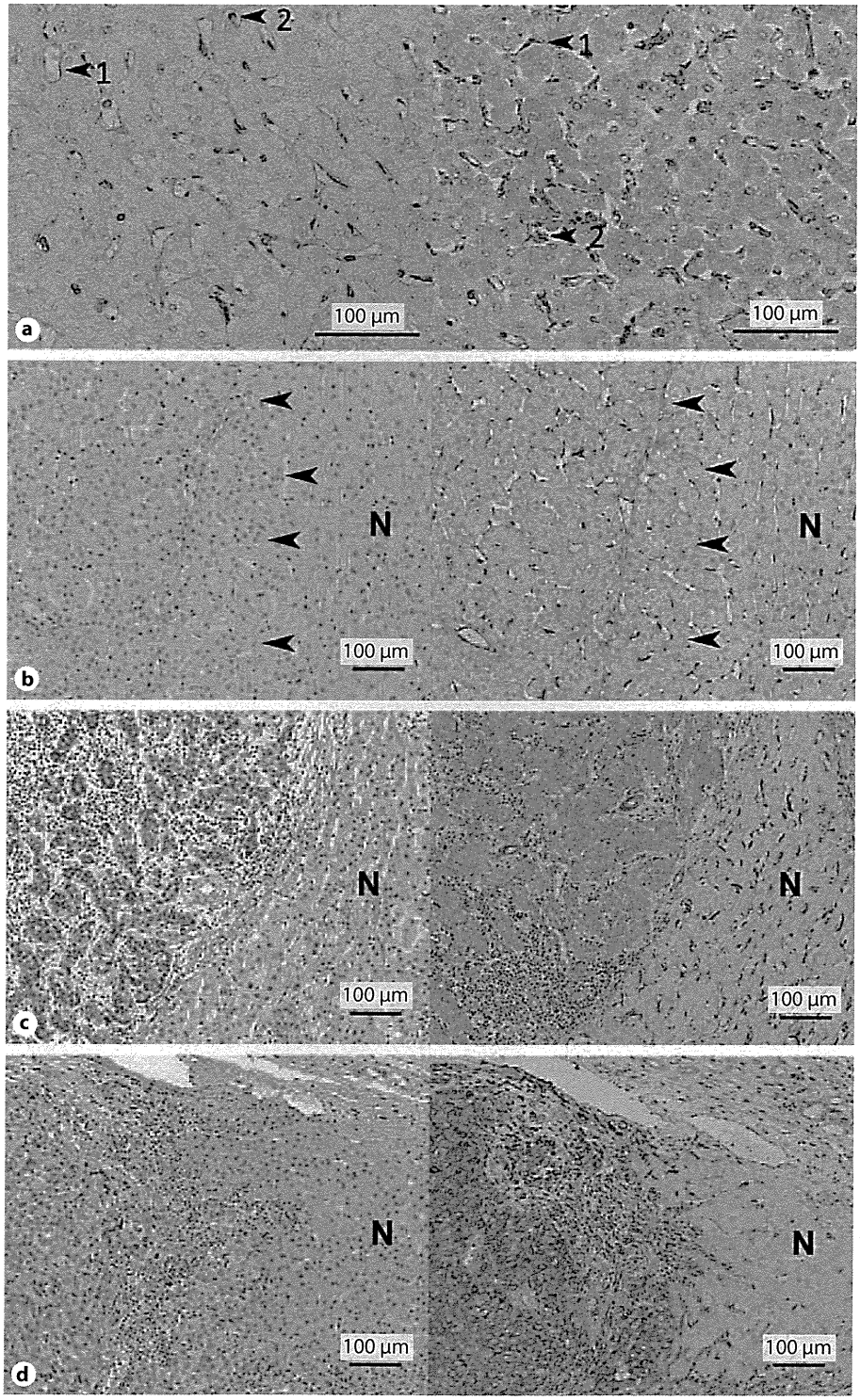

Fig. 2. Immunohistochemical analysis of talin-1. **a** Talin-1 immunostaining of tissue samples used for the proteomic analysis. Left: noncancerous liver tissue. Right: early HCC. Arrowhead 1 indicates a sinusoidal endothelial cell and arrowhead 2 a Kupffer cell. **b–d** Various histological sections were stained with hematoxylin and eosin (left plates) and anti-talin-1 antibody (right plates). **b** An early HCC with slightly stronger staining of talin-1 than the adjacent noncancerous hepatocytes. Arrowheads indicate the borders between early HCC and noncancerous liver (N). **c** A moderately differentiated HCC. **d** A poorly differentiated HCC with very strong staining of talin-1.

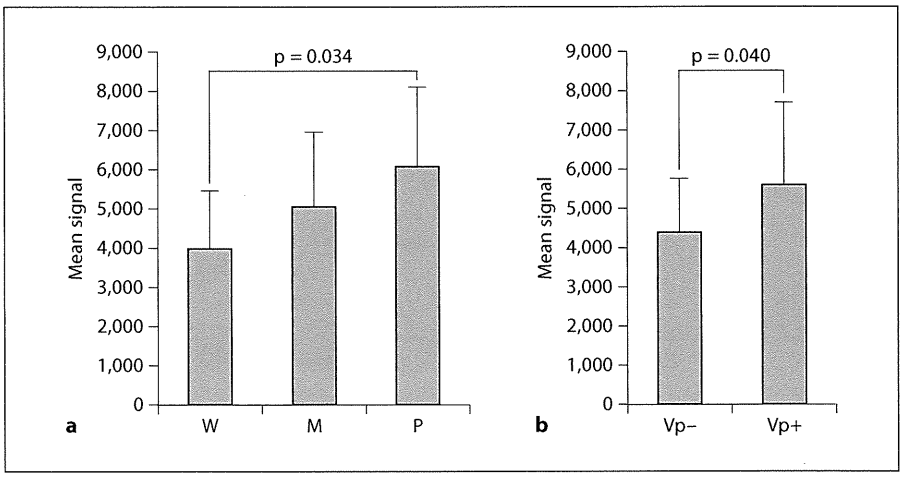

Fig. 3. Microarray analysis. **a** The means of talin-1 mRNA expression in well (W, n = 4), moderately (M, n = 23), and poorly differentiated HCCs (P, n = 13) increased in a stepwise fashion, with a significant difference between well- and poorly differentiated HCCs. **b** The average talin-1 mRNA expression was significantly up-regulated in 28 HCCs with portal vein invasion ('Vp+') as compared to 12 HCCs without portal vein invasion ('Vp–'). Error bars indicate standard deviations.

Table 3. Immunohistochemical reactivity of talin-1 with various histological patterns

Histology	Distribution of the samples according to the percentage of cells with talin-1 upregulation						p value
	<10%	10–30%	30–50%	50–70%	>70%	total	
Dysplastic nodules	4	3	0	1	0	8	
Well-differentiated HCCs (early HCCs)	3 (1)	3 (1)	2 (2)	2 (1)	3 (2)	13 (7)	0.001*
Moderately differentiated HCCs	12	12	11	14	24	73	
Poorly differentiated HCCs	2	0	1	2	15	20	

* Jonckheere-Terpstra test.

cells, which were stained by the anti-talin-1 antibody with remarkable intensity, the immunoreactivity of noncancerous hepatocytes for talin-1 was clearly weak. More intense cytoplasmic staining of the tumor cells by the anti-talin-1 antibody, compared with the adjacent hepatocytes of noncancerous liver, was considered as up-regulation of talin-1 in the tumor cells. The talin-1 immunoreactivities of 8 DNs and 106 HCC nodules are summarized in table 3. Talin-1 was significantly upregulated in early HCC cells compared with adjacent hepatocytes in noncancerous liver (Cochran-Mantel-Haenszel test, p = 0.003). The immunoreactivity of HCCs for talin-1 increased gradually according to the degree of dedifferentiation (fig. 2b–d), with statistical significance (Jonckheere-Terpstra test, p = 0.001). Poorly differentiated HCCs were characterized not only by a high percentage of cancer cells with talin-1 upregulation but also usually by a high intensity of talin-1 staining. DNs were characterized by a significantly lower percentage of talin-1 upregulation compared with all HCCs together (Cochran-Mantel-Haenszel test, p = 0.003).

We investigated the relationship between clinicopathological factors and the expression of talin-1 (table 4). The mean percentage of HCC cells with talin-1 upregulation in the examined 106 HCC nodules was 53%. We divided HCC samples into 2 groups with either more or less than 50% cancer cells showing talin-1 upregulation. As expected, the degree of cell dedifferentiation differed significantly between the 2 groups (Cochran-Mantel-Haenszel test, p = 0.004). Of great interest was the finding that HCCs containing more than 50% cancer cells with talin-1 upregulation had a significantly higher rate of portal vein invasion (Vp) than those with fewer than 50% cancer cells (Fisher's exact test, p = 0.029). In agreement with these results, the review of our past microarray data [14] showed significant upregulation of talin-1 mRNA in poorly differentiated HCCs compared with well-differentiated HCCs (Student's t test, p = 0.034), as well as in

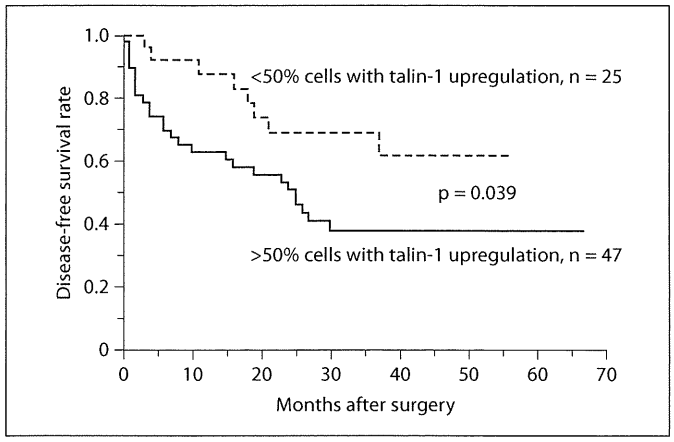

Fig. 4. Kaplan-Meier curves for disease-free survival after surgery. 47 HCC patients with greater talin-1 upregulation (solid line) had a significantly shorter disease-free survival than 25 of those with less talin-1 upregulation (dashed line).

Vp-positive HCCs compared with Vp-negative HCCs ($p = 0.040$) (fig. 3).

During a median follow-up of 25 months (range 0–67), the disease-free survival was analyzed in 72 HCC patients who underwent partial hepatectomy (fig. 4). Setting 50% cancer cells with intense immuno-staining for talin-1 as the threshold, log-rank analysis showed that 47 HCCs with greater talin-1 upregulation had a significantly shorter disease-free survival than 25 of those with less talin-1 upregulation ($p = 0.039$).

Discussion

We applied the latest proteomic technologies to early HCCs and noncancerous tissues derived from native livers of LDLT cases, resulting in identification of talin-1 as a promising candidate marker for HCC progression. In accordance with the proteomic analyses, immunohistochemical examination confirmed talin-1 upregulation in the majority of HCC cells compared with noncancerous hepatocytes. The stepwise increase of immunoreactivity for talin-1 according to the degree of dedifferentiation of HCC suggests the involvement of talin-1 in HCC progression. In general, poor prognosis of progressed HCC is associated with both high rates of intrahepatic metastasis and vascular invasion. The finding that HCCs with upregulation of talin-1 had a significantly higher rate of portal vein invasion might be associated with the shorter time to recurrence after partial hepatectomies for HCCs with talin-1 upregulation, so that the value of talin-1 as a tumor marker may be seen in prediction of clinical outcomes.

Talin-1 is one of several proteins that link the cytoplasmic domains of integrin β subunits to actin filaments [7].

Table 4. Correlations between talin-1 expression and clinical factors

Variables	Distribution of the samples (n[d]) according to the percentage of cells with talin-1 upregulation			p value[e]
	<50%	>50%	total	
Sex				0.599
Male	30	42	72	
Female	6	13	19	
Age				0.510
<60 years	12	23	35	
≥60 years	24	32	56	
Nonviral or viral (HCV + HBV)				0.083
Nonviral	13	10	23	
Viral (HCV + HBV)	23	45	68	
HCV or HBV[a]				0.422
HCV	12	30	42	
HBV	10	15	25	
Background tissue[b]				1.000
Not liver cirrhosis	20	31	51	
Liver cirrhosis	14	22	36	
Histology				0.004
Early/well-differentiated HCC	8	5	13	
Moderately differentiated HCC	35	38	73	
Poorly differentiated HCC	3	17	20	
Portal vein invasion (Vp)[c]				0.029
Vp–	26	21	47	
Vp+	19	39	58	
Intrahepatic metastasis (im)[c]				0.070
im–	38	41	79	
im+	7	19	26	

[a] One case was not counted because of infection with both HCV and HBV. [b] Four cases were not counted because of difficulty in evaluating the histology of the background tissues. [c] One sample was not counted because of difficulty in judging the presence of portal vein invasion and/or intrahepatic metastasis. [d] In the categories 'Sex', 'Age', 'Nonviral or viral', 'HCV or HBV', and 'Background tissue', n indicates the number of cases. When a case had multiple nodules, the highest percentage among the most dedifferentiated nodules was counted. In the categories 'Histology', 'Portal vein invasion', and 'Intrahepatic metastasis', n indicates the number of HCC nodules. [e] All categories were analyzed statistically with Fisher's exact test, except 'Histology' with Cochran-Mantel-Haenszel test.

Binding of talin-1 to β-integrin cytoplasmic domains is thought to trigger a conformational change in the αβ-integrin extracellular domains that increases their affinity for extracellular matrix proteins [18] and promotes assembly of focal adhesions. Talin-1 plays a pivotal role in focal adhesion dynamics, as calpain-2-mediated proteolytic cleavage of talin-1 is a rate-limiting step in focal adhesion disassembly [19]. Interactions between vinculin, talin, and actin filaments appear to constitute a slippage interface between the cytoskeleton and integrins, generating a molecular clutch that is regulated during the morphodynamic transitions of cell migration [20]. Recently, overexpression of talin-1 was reported to promote prostate cancer cell adhesion, migration and invasion [21]. Such knowledge about the cytomorphodynamic roles of talin-1 may be brought in connection with the higher incidence of portal vein invasion in HCCs with talin-1 upregulation. In addition, talin-1 also functions in signal transduction in focal adhesions, as it recruits focal adhesion kinase (FAK), which in turn recruits Src and Ras to activate downstream signaling pathways [22]. It is noteworthy that FAK itself is involved in the metastasis and invasion of HCC [23]. Recently, several molecular-targeted therapies have been developed for the treatment of various malignant diseases, and the multikinase inhibitor sorafenib has shown survival benefits in patients with advanced HCC [24]. Accumulation of knowledge about molecules such as talin-1, which may be involved in carcinogenic signaling pathways, may make available new possibilities for molecular-targeted therapy.

Besides talin-1, the 61 proteins which our proteomic analyses identified as up-regulated in HCC included HSP70, which is known as a molecular marker of HCC [4]. Filamin-A, a cytoskeletal protein listed in table 2, was recently reported to be involved in the metastasis of HCC cells [17]. Our immunohistochemical study, however, did not reveal a significant difference in filamin-A expression between HCC and noncancerous liver (data not shown). The majority of the proteins identified as up-regulated in HCC by our proteomic study still await further validation.

Proteomics has greatly contributed to the identification of specific markers for several human cancers [25]. In this work, we used a high-resolution 2DLC-MS/MS methodology for differential tissue proteome analysis. A characteristic of this strategy lies in the automated alignment of peptide signal data obtained from individual samples, which enables direct comparison of peptide signal intensities among multiple LC-MS/MS runs without any need for isotope labeling [26] and contributes to the increased reliability of analytic results. In addition, proteolytic hydrolysis of the target proteome increases the range of separable protein molecular mass, when compared to the conventional two-dimensional electrophoresis system that is based on the separation of intact proteins by their size/charge and is incapable of detecting high-molecular-mass proteins such as talin-1. It should be noted that perfusion of freshly obtained whole livers with heparinized saline resulted in depletion of body-fluid-derived, high-abundance proteins from the starting materials and, thus, enrichment of tissue proteins in the analyte. With the use of appropriately prepared materials, advanced differential tissue proteomics has the potential to detect quantitative changes of low-abundance tissue proteins which may be the key to carcinogenesis.

In conclusion, talin-1 is significantly upregulated in HCC according to tumor progression and may serve as a prognostic marker. Advanced proteomic techniques applied to freshly obtained whole native livers including early HCC portions may be a powerful method to identify unknown molecules involved in hepatocarcinogenesis.

Acknowledgements

The authors would like to thank Dr. Takeshi Kawamura, Tokyo Medical University, for his insightful supports and comments. Ms. Hisae Anyoji and Mr. Kazuya Wada, Medical Proteo-Scope Co., made enormous contributions to the analysis of the proteomics data. Special thanks also to Mr. Shinji Sato, Maze Inc., Tokyo, Japan, for his technical support of the identical sequence counting.

References

1 Takayama T, Makuuchi M, Hirohashi S, Sakamoto M, Okazaki N, Takayasu K, Kosuge T, Motoo Y, Yamazaki S, Hasegawa H: Malignant transformation of adenomatous hyperplasia to hepatocellular carcinoma. Lancet 1990;336:1150–1153.

2 Takayama T, Makuuchi M, Hirohashi S, Sakamoto M, Yamamoto J, Shimada K, Kosuge T, Okada S, Takayasu K, Yamasaki S: Early hepatocellular carcinoma as an entity with a high rate of surgical cure. Hepatology 1998;28:1241–1246.

3 International Consensus Group for Hepatocellular Neoplasia: Pathologic diagnosis of early hepatocellular carcinoma: a report of the international consensus group for hepatocellular neoplasia. Hepatology 2009;49:658–664.

4 Chuma M, Sakamoto M, Yamazaki K, Ohta T, Ohki M, Asaka M, Hirohashi S: Expression profiling in multistage hepatocarcinogenesis: identification of HSP70 as a molecular marker of early hepatocellular carcinoma. Hepatology 2003;37:198–207.
5 Shibata R, Mori T, Du W, Chuma M, Gotoh M, Shimazu M, Ueda M, Hirohashi S, Sakamoto M: Overexpression of cyclase-associated protein 2 in multistage hepatocarcinogenesis. Clin Cancer Res 2006;12:5363–5368.
6 McDonald WH, Yates JR 3rd: Shotgun proteomics: Integrating technologies to answer biological questions. Curr Opin Mol Ther 2003;5:302–309.
7 Critchley DR: Cytoskeletal proteins talin and vinculin in integrin-mediated adhesion. Biochem Soc Trans 2004;32:831–836.
8 Maeda J, Hirano T, Ogiwara A, Akimoto S, Kawakami T, Fukui Y, Oka T, Gong Y, Guo R, Inada H, Nawa K, Kojika M, Suga Y, Ohira T, Mukai K, Kato H: Proteomic analysis of stage I primary lung adenocarcinoma aimed at individualisation of postoperative therapy. Br J Cancer 2008;98:596–603.
9 Hibi T, Mori T, Fukuma M, Yamazaki K, Hashiguchi A, Yamada T, Tanabe M, Aiura K, Kawakami T, Ogiwara A, Kosuge T, Kitajima M, Kitagawa Y, Sakamoto M: Synuclein-gamma is closely involved in perineural invasion and distant metastasis in mouse models and is a novel prognostic factor in pancreatic cancer. Clin Cancer Res 2009;15:2864–2871.
10 Fujii K, Nakano T, Kanazawa M, Akimoto S, Hirano T, Kato H, Nishimura T: Clinical-scale high-throughput human plasma proteome analysis: lung adenocarcinoma. Proteomics 2005;5:1150–1159.
11 Marko-Varga G, Ogiwara A, Nishimura T, et al: Personalized medicine and proteomics: lessons from non-small cell lung cancer. J Proteome Res 2007;6:2925–2935.
12 Perkins DN, Pappin DJ, Creasy DM, Cottrell JS: Probability-based protein identification by searching sequence databases using mass spectrometry data. Electrophoresis 1999;20:3551–3567.
13 Hsu SM, Raine L, Fanger H: Use of avidin-biotin-peroxidase complex (ABC) in immunoperoxidase techniques: a comparison between ABC and unlabeled antibody (PAP) procedures. J Histochem Cytochem 1981;29:577–580.
14 Chuma M, Saeki N, Yamamoto Y, Ohta T, Asaka M, Hirohashi S, Sakamoto M: Expression profiling in hepatocellular carcinoma with intrahepatic metastasis: Identification of high-mobility group I(Y) protein as a molecular marker of hepatocellular carcinoma metastasis. Keio J Med 2004;53:90–97.
15 Hall A: The cytoskeleton and cancer. Cancer Metastasis Rev 2009;28:5–14.
16 Yamazaki K, Takamura M, Masugi Y, Mori T, Du W, Hibi T, Hiraoka N, Ohta T, Ohki M, Hirohashi S, Sakamoto M: Adenylate cyclase-associated protein 1 overexpressed in pancreatic cancers is involved in cancer cell motility. Lab Invest 2009;89:425–432.
17 Ai J, Huang H, Lv X, Tang Z, Chen M, Chen T, Duan W, Sun H, Li Q, Tan R, Liu Y, Duan J, Yang Y, Wei Y, Li Y, Zhou Q: FLNA and PGK1 are two potential markers for progression in hepatocellular carcinoma. Cell Physiol Biochem 2011;27:207–216.
18 Calderwood DA: Integrin activation. J Cell Sci 2004;117:657–666.
19 Franco SJ, Rodgers MA, Perrin BJ, Han J, Bennin DA, Critchley DR, Huttenlocher A: Calpain-mediated proteolysis of talin regulates adhesion dynamics. Nat Cell Biol 2004;6:977–983.
20 Hu K, Ji L, Applegate KT, Danuser G, Waterman-Storer CM: Differential transmission of actin motion within focal adhesions. Science 2007;315:111–115.
21 Sakamoto S, McCann RO, Dhir R, Kyprianou N: Talin1 promotes tumor invasion and metastasis via focal adhesion signaling and anoikis resistance. Cancer Res 2010;70:1885–95.
22 Chen HC, Appeddu PA, Parsons JT, Hildebrand JD, Schaller MD, Guan JL: Interaction of focal adhesion kinase with cytoskeletal protein talin. J Biol Chem 1995;270:16995–16999.
23 Chen JS, Huang XH, Wang Q, Chen XL, Fu XH, Tan HX, Zhang LJ, Li W, Bi J: FAK is involved in invasion and metastasis of hepatocellular carcinoma. Clin Exp Metastasis 2010;27:71–82.
24 Llovet JM, Bruix J: Molecular targeted therapies in hepatocellular carcinoma. Hepatology 2008;48:1312–1327.
25 Hanash SM, Pitteri SJ, Faca VM: Mining the plasma proteome for cancer biomarkers. Nature 2008;452:571–579.
26 America AH, Cordewener JH: Comparative LC-MS: a landscape of peaks and valleys. Proteomics 2008;8:731–749.